Parallel electron-hole bilayer conductivity from electronic interface reconstruction

R. Pentcheva,[1] M. Huijben,[2] K. Otte,[1] W.E. Pickett,[3] J.E. Kleibeuker,[2] J. Huijben,[2] H. Boschker,[2] D. Kockmann,[2] W. Siemons,[4] G. Koster,[2] H.J.W. Zandvliet,[2] G. Rijnders,[2] D.H.A. Blank,[2] H. Hilgenkamp,[2] and A. Brinkman[2]

[1]*Department of Earth and Environmental Sciences, Section Crystallography, University of Munich, Germany*
[2]*Faculty of Science and Technology and MESA$^+$ Institute for Nanotechnology, University of Twente, The Netherlands*
[3]*Department of Physics, University of California, Davis, USA*
[4]*Department of Physics, University of California, Berkeley, USA*
(Dated: December 22, 2009)

The perovskite SrTiO$_3$-LaAlO$_3$ structure has advanced to a model system to investigate the rich electronic phenomena arising at polar interfaces. Using first principles calculations and transport measurements we demonstrate that an additional SrTiO$_3$ capping layer prevents structural and chemical reconstruction at the LaAlO$_3$ surface and triggers the electronic reconstruction at a significantly lower LaAlO$_3$ film thickness than for the uncapped systems. Combined theoretical and experimental evidence (from magnetotransport and ultraviolet photoelectron spectroscopy) suggests two spatially separated sheets with electron and hole carriers, that are as close as 1 nm.

Electronic reconstruction [1] at the SrTiO$_3$ (STO) - LaAlO$_3$ (LAO) interface [2–4] and the resulting electronic transport properties [5–10] are based on the polar nature of LAO. The polarity of LAO arises from the LaO and AlO$_2$ layers being not charge neutral in the [001] direction, unlike the formally neutral TiO$_2$ and SrO layers of STO. In the ionic limit, LaO has a charge $q = +e$ and AlO$_2$ $q = -e$ per unit cell. The screened dipole per unit cell is then $D = q\Delta z/\epsilon$, where the spacing $\Delta z = c/2$ ($c = 3.9$ Å is the out of plane lattice parameter) and $\epsilon = 25$ is the dielectric constant of LAO [11]. Screening contributions come primarily from a strong lattice polarization of the LAO film (these can be as high as $\sim 62\%$ [12]), supplemented by electronic cloud deformation [13]. For STO-LAO systems, the remaining screened dipole of 0.08 eÅ per cell is expected to give rise to an internal electric field of 2.4×10^7 V/cm, and a resulting build-up of electric potential of 0.9 V per LAO unit cell.

This potential shift explains quantitatively why, above a threshold of 3-4 unit cells, electrons are transferred from the surface, across the LAO slab, into the STO conduction band. The resulting insulator-to-metal transition has been observed experimentally for the n-type LaO/TiO$_2$-interface [6]. However, the corresponding potential shifts across LAO have not been detected so far in experiments. For a reconstructed STO-LAO interface, it should be noted that also the LAO surface itself needs to reconstruct to avoid potential build-up, either structurally, electronically, or chemically. After electronic charge transfer one would expect holes at the surface, which have also never been observed.

In this Letter we show that an additional STO capping layer circumvents structural and chemical reconstructions at the LAO surface. An O $2p$ band shift in the STO capping allows for hole doping, so that an electronic reconstruction mechanism comes into play. By means of the STO capping layer one enters a new regime in the field of electronically reconstructed oxide interfaces with two spatially separated 2D conducting sheets, one electron-like and the other hole-like, that can display new electronic behavior including the possibility of a 2D excitonic liquid phase.

The system consisting of a varying number of LAO monolayers (ML), $n = 1 - 5$ ML, and of a STO capping layer, $m = 0 - 2$ ML, stacked on an STO(001) substrate, was studied by density functional theory (DFT) calculations [14] in the generalized gradient approximation (GGA) [15] (for details on the calculations see Ref.[12]). The calculated layer-resolved densities of states are presented in Fig. 1a for 2ML LAO with and without 1ML STO capping. The effect of the electric field within the LAO film is apparent from the shifts of bands, *e.g.* by ~ 0.4 eV per LAO unit cell for the uncapped system [12].

Adding a single unit-cell STO capping layer is found to have a dramatic impact on the calculated electronic structure: the band gap, being 1.2 eV for STO(001)/2LAO, is nearly closed for STO(001)/2LAO/1STO. The evolution of the band structure of STO(001)/2LAO/mSTO with increasing number of capping layers ($m = 0 - 2$) is depicted in Fig. 1b. The valence band maximum is defined by the O $2p$-states at the M(π,π)-point in the surface layer, while Ti $3d$-states at Γ at the n-type interface mark the bottom of the conduction band. In the capped systems a dispersive O $2p$ surface band extends 0.8 eV above the subsurface O $2p$ band and effectively reduces the band gap driving the insulator-to-metal transition at an LAO thickness of only 2ML compared to 4 ML in the uncapped case. This surface state is analogous to the one on the clean STO (001) surface [17, 18]. Further STO layers (*e.g.* STO(001)/2LAO/2STO and STO(001)/3LAO/1STO [16]) increase the band overlap at the Fermi level, but have an overall weaker influence due to the lack of internal field in STO.

While the ionic relaxation pattern [12] changes drastically when a capping layer is added [16], the net contribution of the TiO$_2$ and SrO layers does not affect appreciably the total ionic dipole moment of the film (which scales with the number of LAO layers), and the gap reduction cannot be explained by this difference in ionic displacements. The reduction of the band gap, and finally its closing, is due to three *electronic* effects: (i) the steady upward shift of the O $2p$ states as they approach the surface [12], (ii) the band discontinuity at the interface between LAO and the capping STO layer, and (iii) a
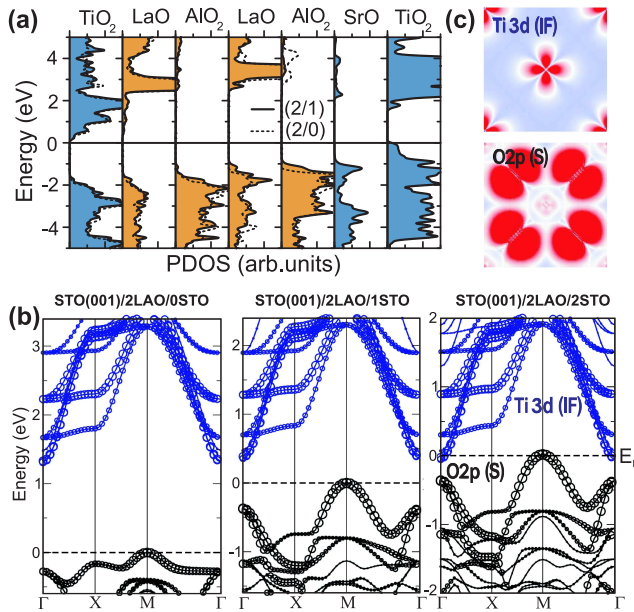
FIG. 1: (a) Layer-resolved density of states (DOS) of STO(001)/2LAO (dotted line), and STO(001)/2LAO/1STO (black line, colored area) aligned at the bottom of the Ti $3d$ band at the interface. (b) Influence of the STO capping on the band structure of STO(001)/2LAO/mSTO with increasing number of capping layers ($m = 0 - 2$), showing the closing of the band gap due to overlap between surface O $2p$ states (black circles) and interface Ti $3d$ states (blue circles). (c) The electron density distribution in the TiO_2 layers of the $m = 2$ sample displays electrons in the Ti $3d_{xy}$ orbitals at the interface (top) and holes in the O $2p_\pi$ bands at the surface (bottom). The electron density is integrated between -0.6 and 0.0 eV.
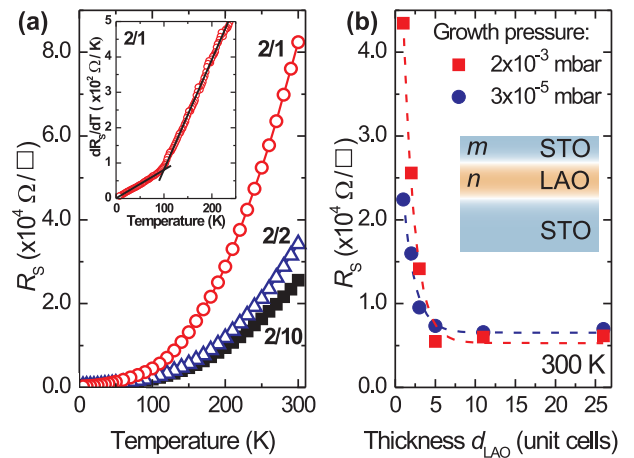

FIG. 2: (a) Sheet resistance as a function of temperature for three different STO-LAO-STO samples: STO(001)/2LAO/1STO (red circles), STO(001)/2LAO/2STO (blue triangles), and STO(001)/2LAO/10STO (black squares). The sample of STO(001)/2LAO was found to be insulating. All samples are grown at 2×10^{-3} mbar of oxygen. Inset: dR/dT as a function of temperature with different linear fits below and above 100 K. (b) Sheet resistance at room temperature of STO(001)/nLAO/10STO samples for varying LAO interlayer thickness and a fixed number of 10 unit cells of the STO capping layer. Red squares indicate samples grown at relatively high oxygen pressure (2×10^{-3} mbar), blue circles indicate samples grown at lower oxygen pressure (3×10^{-5} mbar).

dispersive O $2p$ surface band in the capped systems that extends 0.8 eV above the subsurface O $2p$ band.

Experimentally, we confirm the crucial influence of a single monolayer of nonpolar material on the electronic interface reconstruction. STO(001)/nLAO/mSTO samples were made by pulsed laser deposition of n ML of LAO and m ML of STO on TiO_2-terminated STO(001) substrates (for fabrication details, see Ref. 5, 8). While uncapped STO(001)/2LAO samples are found to be insulating (sheet resistance above 1 GΩ/□), samples with an additional single ML of STO are conducting (see Fig. 2a). The conductivity is further enhanced in STO(001)/2LAO/2STO samples, but the influence of increasing the STO capping layer thickness weakens, as expected from the DFT results: the STO(001)/2LAO/10STO sample has almost the same conductivity as the STO(001)/2LAO/2STO sample. Samples with a single ML of LAO were found to be insulating except for the sample with a thick STO capping ($m \geq 10$).

It is known that the sheet resistance in STO/LAO samples depends critically on the oxygen pressure during growth [8, 19–22] and can vary over many orders of magnitude [8]. Figure 2b shows the sheet resistance for two different sets of STO/LAO/STO heterostructures with varying LAO inter-

layer thickness, grown at a relatively high oxygen pressure (2×10^{-3} mbar) and at lower oxygen pressure (3×10^{-5} mbar). For the coupled-interface samples, the influence of the oxygen pressure is now found to be much weaker. Apparently, the STO capping protects the underlying LAO surface against reconstruction via defects or adsorbates and provides a way to probe the nature of the *electronic* interface reconstruction.

In analogy to $BaTiO_3$, it is expected [18] that the upward shift of the surface valence band of STO is largest at $T < 105$ K, i.e. below the cubic-to-tetragonal transition [23]. In order to obtain spectroscopic evidence for the reconstruction scenario with the additional temperature dependent STO surface band shift, ultraviolet photoelectron spectroscopy (UPS) was performed *in situ* immediately after the growth of a STO(001)/2LAO/1STO sample. The spectra are shown in Fig. 3 for various temperatures and detection angles. While the overall spectra (see inset of Fig. 3a) resemble those for bulk STO [24], a clear 1 eV peak shift to higher binding energy is observed for 80 K when compared to 300 K. This can be interpreted as an upward shift of the Fermi energy relative to the valence band maximum in the bulk of STO when lowering the temperature.

The spectra taken at lower detector angles are more surface sensitive. Figure 3b shows the gradual increase of density of states towards the sample surface at energies between the bulk STO valence band edge and the Fermi energy. These states
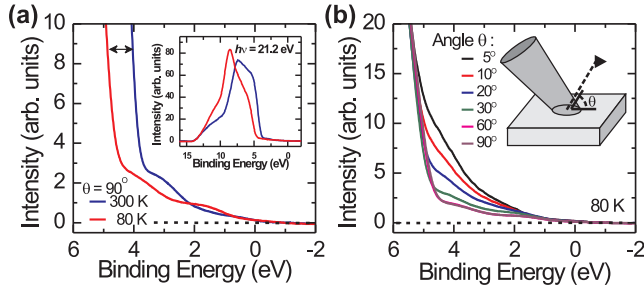
FIG. 3: (a) UPS spectra of a STO(001)/2LAO/1STO sample taken *in situ* after growth, at 300 K and 80 K with the detector at 90°. The inset shows the zoomed-out full spectra. The data has been normalized to the integrated peak height. The arrows indicate a significant shift of about 1 eV that was observed between the spectra. (b) UPS spectra at 80 K under various detector angles (the inset shows how the angle is defined). A gradual filling of the valence band towards the Fermi energy is shown for lower angles. Lower angle spectra have larger contributions from the surface layers.
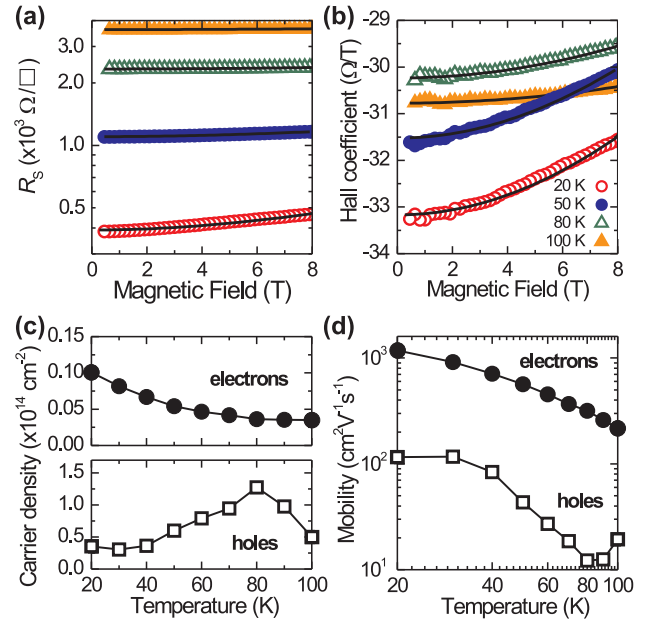

FIG. 4: (a) Sheet resistance as function of magnetic field at different temperatures for a STO(001)/2LAO/1STO sample, exhibiting a positive magnetoresistance. (b) Hall coefficient (R_H/H) of the same sample as a function of magnetic field. (c) Sheet carrier densities and (d) mobilities as obtained from a two-band fit to the magnetoresistance and Hall data at each temperature.

originate from the valence band of LAO as well as the valence band of the STO surface layer. Note, that the valence band states penetrate all the way to the Fermi energy, unlike studies on doped-STO [25], where only trapped states close to the conduction band are usually observed. The STO surface state induced Fermi level shift as well as the observed density of states at the Fermi energy (Fig. 1) are consistent with the reconstruction scenario and imply the presence of holes in transport. Further spectroscopic evidence for this scenario is provided by scanning tunneling spectroscopy [16].

To investigate the possibility of a parallel electron-hole bilayer and the sign of the charge carriers in capped systems, magnetoresistance and Hall data were analyzed. Because the intrinsic coupling between the layers would not allow to probe the transport properties of the layers individually, unless structures are realized on a sub-micron length scale, our measurements contain information on the layers in parallel. Fig. 4 displays a positive non-quadratic magnetoresistance and a Hall resistance whose slope increases for higher fields for all conducting STO/LAO/STO samples. Quantum oscillations can still be excluded because of the low mobility. A negative magnetoresistance contribution observed for single-interface samples deposited at high oxygen pressure [8] only appears below 10 K. It is, therefore, natural to interpret the observations in terms of multiband conductivity. Indeed, in the temperature range up to 100 K, the magnetoresistance as well as the Hall resistance can be fitted (solid lines in Fig. 4 a and b) with a two band model [16]. Two carrier concentrations and two mobilities could be obtained for the STO(001)/2LAO/1STO sample from fitting as a function of temperature (Fig. 4 c and d).

The positive carrier sign of one of the bands at low temperatures indicates hole-type conductivity, while the other band is of electron-type. We note that no fit to the data could be obtained for equal signs of the two carrier densities. Neither oxygen vacancy doping, nor doping by cation substitu-

tion, have ever been shown to give rise to hole conductivity in the STO/LAO system. The calculated electron density distribution in Fig. 1c displays electrons of Ti $3d_{xy}$ orbital character in the interface TiO$_2$ layer, while holes of O $2p_\pi$ type are present in the surface TiO$_2$ layer. Consequently, we attribute the hole band to the surface layer, while the electron band, with a lower carrier density but a much larger mobility, is naturally attributed to the Ti $3d_{xy}$ states [26] at the interface to the substrate.

Note, that the hole density is about an order of magnitude larger than the electron density. However, the Hall effect is dominated by the electron band because of its large mobility (10^3 cm^{2}V^{-1}s^{-1}, similar to values obtained on single interface STO/LAO samples deposited at oxygen pressures $> 10^{-3}$ mbar). The unequal number of electrons and holes illustrates that not all charge carriers are visible in transport measurements. While the effective electron and hole masses cannot be directly inferred from our data, the band structure calculations (neglecting strong correlation effects and defects) render 0.4 m_e for the electrons (both in the capped and uncapped system) and a significantly higher effective mass of holes (1.4 m_e in the uncapped system) which is reduced to 1.2 m_e in the capped case.

Above 100 K, neither magnetoresistance, nor a nonlinear Hall resistance are observed. At these high temperatures the mobilities become so low that no magnetoresistance effects are expected anyway ($\mu^2H^2 \ll 1$ in the two-band equations as

described in [16]). The disappearance of the two-band effects is also consistent with the $R_S(T)$ behavior changing around this temperature (see the inset of Fig. 2a), and the expectation that no electronic reconstruction has yet taken place above 105 K for this sample.

However, at $T > 100$ K conductivity also occurs, suggesting that some additional carriers are already present at the interface before electronic reconstruction has taken place. The additional carriers can originate from vacancies or cation interdiffusion that contribute to the screening of the potential build-up during the growth of LAO. One important observation in this respect is shown in [16], where the two-band fitting results are depicted for a large number of samples with either thicker LAO or capping STO. While theory predicts for defect-free systems an increase in the band overlap, and hence in the number of electrons and holes, no hole contribution was found any longer experimentally beyond $n = 2$ and $m = 1$. A possible scenario is that non-electronic contributions to reconstruction occur during the growth of LAO or STO when the potential build-up exceeds a certain value, also giving rise to interfacial conductivity. The STO(001)/2LAO/1STO might then be an example of a structure where the potential build-up during growth is not yet large enough for a complete non-electronic reconstruction. Only upon cooling down below 105 K, where an additional potential shift occurs (and where temperature is too low to create structural reconstruction) is there a need for additional electronic reconstruction, explaining the observation of electrons and holes. This scenario provides guidelines to enhancing electronic reconstruction effects in general.

The STO capping has enabled us to show that holes are present in reconstructed oxide interface samples. The mobility is low and it is expected that the holes can become localized or eliminated in uncapped STO/LAO systems more strongly (*e.g.* by absorbed molecules or by ionic surface reconstruction). This possibly explains the large sensitivity of uncapped samples to growth conditions and the possibility to manipulate the interface conductivity by an atomic force microscope tip [27, 28].

As shown in Fig. 1 The surface valence band has its maximum at the M=(π, π) zone corner, whereas the substrate-LAO interface conduction band has its minimum at the zone center. This makes the band overlap distant not only in real space (across 12 Å or more, depending on capping layer thickness) but also indirect in momentum. As a practical consequence, an electron at the surface cannot move to the substrate without any mechanism to supply the momentum transfer. The obvious mechanism is via phonons, specifically M=(π, π) phonons. These are zone boundary optical phonons, which typically lie at a few tens of meV energy. Equilibration of electrons and holes across the LAO slab will be slow at low temperature, but will occur rapidly as soon as optical phonons are excited.

A further consequence of this 2D electron-hole bilayer is that it provides the conditions necessary for formation of a 2D excitonic liquid [29, 30] comprised of interacting indirect excitons. In this oxide nanostructure the separation of the 2D electron and hole gases can be varied by the choice of polar material as well as capping material. In analogy to other oxides, such as ZnO [31], it is expected that higher mobilities can be obtained by reducing the defect density. Furthermore, the carrier densities can be tuned by gating, allowing a substantial parameter range to be probed.

[1] R. Hesper, L. H. Tjeng, A. Heeres, and G. A. Sawatzky, Phys. Rev. B **62**, 16046 (2000).
[2] A. Ohtomo and H. Y. Hwang, Nature **427**, 423 (2004).
[3] A. Ohtomo and H. Y. Hwang, Nature **441**, 120 (2006).
[4] N. Nakagawa, H. Y. Hwang, and D. A. Muller, Nature Mater. **5**, 204 (2006).
[5] M. Huijben *et al.*, Nature Mater. **5**, 556 (2006).
[6] S. Thiel, G. Hammerl, A. Schmehl, C. W. Schneider, and J. Mannhart, Science **313**, 1942 (2006).
[7] N. Reyren *et al.*, Science **317**, 1196 (2007).
[8] A. Brinkman *et al.*, Nature Mater. **6**, 493 (2007).
[9] A. D. Caviglia *et al.*, Nature **456**, 624 (2008).
[10] M. Basletić *et al.*, Nature Mater. **7**, 621 (2008).
[11] S. A. Hayward *et al.*, Phys. Rev. B **72**, 054110 (2005).
[12] R. Pentcheva and W. E. Pickett, Phys. Rev. Lett. **102**, 107602 (2009).
[13] S. Ishibashi and K. Terakura, J. Phys. Soc. Jpn. **77**, 104706 (2008).
[14] P. Blaha, K. Schwarz, G.K.H. Madsen, and J. Luitz, (K. Schwarz, Techn. Univ. Wien, Austria), ISBN 3-9501031-1-2 (2001).
[15] J. P. Perdew, K. Burke, and M. Ernzerhof, Phys. Rev. Lett. **77**, 3865 (1996).
[16] See EPAPS information.
[17] S. Kimura, J. Yamauchi, M. Tsukada, and S. Watanabe, Phys. Rev. B **51**, 11049 (1995).
[18] J. Padilla and D. Vanderbilt, Surf. Sci. **418**, 64 (1998).
[19] W. Siemons *et al.*, Phys. Rev. Lett. **98**, 196802 (2007).
[20] G. Herranz *et al.*, Phys. Rev. Lett. **98**, 216803 (2007).
[21] A. Kalabukhov *et al.*, Phys. Rev. B **75**, 121404(R) (2007).
[22] M. Huijben *et al.*, Adv. Mater. **21**, 1665 (2009).
[23] J. Padilla and D. Vanderbilt, Phys. Rev. B **56**, 1625 (1997).
[24] W. Siemons *et al.*, Phys. Rev. B **76**, 155111 (2007).
[25] W. Maus-Friedrichs *et al.*, Surf. Sci. **515**, 499 (2002).
[26] M. Salluzzo *et al.*, Phys. Rev. Lett. **102**, 166804 (2009).
[27] C. Cen *et al.*, Nature Mater. **7**, 298 (2008).
[28] C. Cen, S. Thiel, J. Mannhart, and J. Levy, Science **323**, 1026 (2009).
[29] L. V. Keldysh and Y. V. Kopaev, Sov. Phys. JETP **6**, 2219 (1965).
[30] J. des Cloizeaux, J. Phys. Chem. Solids **26**, 259 (1965).
[31] A. Tsukazaki *et al.*, Science **315**, 1388 (2007).